Physiological Measurement

PAPER

Novel instrumental markers of proximal scleroderma provided by imaging photoplethysmography

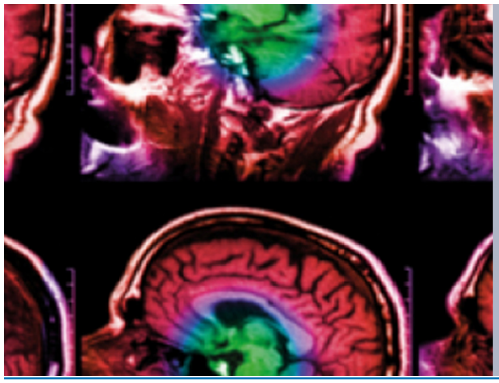

IOP Publishing Physiol. Meas. 41 (2020) 044004 https://doi.org/10.1088/1361-6579/ab807c

Physiological Measurement

IPEM Institute of Physics and Engineering in Medicine

PAPER

Novel instrumental markers of proximal scleroderma provided by imaging photoplethysmography

RECEIVED
28 August 2019

REVISED
29 January 2020

ACCEPTED FOR PUBLICATION
17 March 2020

PUBLISHED
1 May 2020

Oleg V Mamontov[1,2], Tatiana V Krasnikova[1,2], Maxim A Volynsky[2], Natalia A Anokhina[3], Evgeny V Shlyakhto[4] and Alexei A Kamshilin[2]

[1] Department of Circulation Physiology, Almazov National Medical Research Centre, St. Petersburg, Russia
[2] Faculty of Applied Optics, ITMO University, St. Petersburg, Russia
[3] Department of Rheumatology, Almazov National Medical Research Centre, St. Petersburg, Russia
[4] Institute of Cardiovascular Diseases, Almazov National Medical Research Centre, St. Petersburg, Russia

E-mail: alexei.kamshilin@yandex.ru

Keywords: imaging photoplethysmography, proximal scleroderma, pulse transit time

Abstract

Objective: Instrumental identification of proximal scleroderma, which is necessary for the early diagnosis of systemic sclerosis (SSD), has not yet been developed. The aim of this study was to assess the potential diagnostic value of the imaging photoplethysmography (IPPG) method in patients with SSD. *Approach*: The study enrolled 19 patients with SSD and 21 healthy subjects matched by age and sex with the patients. Spatial distribution of capillary-blood-flow parameters and their dynamics was estimated in the facial area of patients and subjects. In the IPPG system, a 40 s video of the subject's face illuminated by green polarized light was recorded with a monochrome digital camera in synchronization with the electrocardiogram. Experimental data were processed using custom software allowing assessment of an arrival time of the blood pressure wave (PAT), an amplitude of pulsatile component (APC) of the photoplethysmographic (PPG) waveform, and their variability. *Main results*: Our study has revealed a significant increase in PAT variability in patients with SSD compared to the control group: 52 ± 47 ms vs 24 ± 13 ms ($P = 0.01$). Similarly, the variability of the PPG-pulse shape was larger in patients with SSD: $0.13 \pm 0.07\%$ vs $0.09 \pm 0.02\%$ ($P < 0.001$). In addition, patients with scleroderma showed a significantly greater degree of asymmetry of the APC parameter than the control group: 17.7 ± 9.7 vs 7.9 ± 5.0 ($P < 0.001$). At the same time, no correlation was found between the PPG waveform parameters and either the form or duration of the disease. Also, no relationship between the characteristics of the PPG waveform and the modified Rodnan skin score was found. *Significance*: Novel instrumental markers found in our pilot study showed that the IPPG method can be used for diagnosing SSD in the early stages of the disease.

1. Introduction

Systemic sclerosis (SSD) is heavy system disease of connecting tissues that leads to irreversible damage of internal organs and invalidation (Fett 2013). Disease consequences are much more profound in the case of late diagnosis. The earlier pathogenic therapy is started, the more effective the prevention of organ lesions. However, sclerosis diagnosis is based mainly on clinical criteria that involves a large percentage of subjectivism (van der Hoogen *et al* 2013). The only 'major diagnostic criterion' of proximal scleroderma (PSD) is established on the basis of a visual assessment of the skin proximal to the wrist joint. However, visual signs of the scleroderma is far from an early disease indication because their appearance becomes noticeable at an advanced stage of the disease (Leroy and Medsger 2001). Since the sclerosis is based on lesions of both the skin capillaries and internal organs (Furue *et al* 2017, Singh *et al* 2019), the detection of the former can facilitate the diagnosis of the disease. The current technology of capillaroscopy allows assessment of the state of nailfold capillaries only. However, this organ is located distal to the wrist joints. Therefore, it visualizes a small diagnostic sign (van der Hoogen *et al* 2013).

Table 1. Clinical characterization of patients with SSD.

Indication	Form	Number (%)
Clinical form	Diffuse SSD	5 (26%)
	Limited SSD	14 (74%)
	Overlapped syndrome SSD	12 (63%)
	Visceral SSD	13 (68%)
Disease activity	Moderate	18 (95%)
	High	1 (5%)
Duration, years.		8.6 ± 7.5
Body mass index, kg m^{-2}		26.0 ± 6.4
Systolic blood pressure, mmHg		119 ± 11
Diastolic blood pressure, mmHg		78 ± 9
Rodnan score		8.2 ± 5.3

The technology of imaging photoplethysmography (IPPG) at green light allows assessment of the state of capillary blood flow in various areas of the skin (Kamshilin *et al* 2018a, 2018b). For vital sign extraction, the facial area is the most frequently used in IPPG systems because it exhibits a higher signal-to-noise (SNR) ratio than other body parts (Poh *et al* 2010, Kamshilin *et al* 2016, Prakash and Tucker 2018). As is known, lesions in this area often occur with scleroderma. Therefore, it can be detected by using an IPPG system. The main parameters measured in an IPPG system synchronized with the electrocardiogram (ECG) recordings are spatial distributions of (i) the amplitude of the pulsatile component (APC), and (ii) pulse transit time (PTT) in its way between the heart and facial area (Kamshilin *et al* 2016).

The aim of this study was to assess the diagnostic value of IPPG for the diagnosis of PSD. Since synchronous IPPG-ECG recordings allow measurement of both the amplitude and temporal parameters of the photoplethysmographic (PPG) waveforms simultaneously in large areas of the body, we suggest using statistics of these parameters as additional indicators characterizing capillary blood flow.

2. Patients and methods

2.1. Patients and control group

The study enrolled 19 patients with SSD. The mean age of the patients with SSD was 48.4 ± 11.7 years. Among them, 17 patients had a definite diagnosis of SSD, whereas the diagnosis was presumptive in two of them because there were no signs of PSD. Clinical characteristics of the patients (17 female and two male) are presented in table 1. As seen, the majority of patients had limited forms of scleroderma and damage to internal organs. Additionally, most of them had an overlapped syndrome. Almost all patients had moderate disease activity, the average duration of which was about nine years. The severity of skin lesions was assessed using a modified Rodnan skin count, the mean of which was slightly more than eight units. The control group consisted of 21 healthy volunteers matched by age and sex with patients with SSD.

All patients included in the study underwent inpatient treatment in the rheumatology department of the Almazov National Medical Research Centre, St. Petersburg, Russia. Before the study, both the patients and volunteers gave their written informed consent for participation in the experiment in the form approved by the local ethics committee of the Almazov Centre.

2.2. Experimental protocol and arrangement

Parameters of blood flow in the facial area were measured using a custom-made IPPG system synchronized with a digital electrocardiograph (model KAP-01-'Kardiotekhnika-EKG', Incart Ltd.). The IPPG system was described in detail previously (Kamshilin *et al* 2018a). Briefly, it consisted of a digital monochrome CMOS camera (8-bit model GigE uEye UI-5220SE, Imaging Development Systems, GmbH) and a light-emitting diode (LED) source with a polarization filter. Video recording of the subject's facial area was carried out in the sedentary position over 40 s. A subject was asked to sit comfortably, breathe normally, avoid any movement, and lean his head on a properly adjusted support. To implement ECG recordings, disposable electrodes were attached to the left and right wrists with the reference electrodes on the legs. We used two leads to collect ECG data. Synchronization accuracy between the electrocardiograph and the camera was better than 1 ms.

The subject's face was illuminated by eight green LEDs (wavelength of 525 ± 40 nm, power of 8×3 W) assembled around the camera lens. Specular reflections were avoided by using a cross-polarization filter (Sidorov *et al* 2016) consisting of an inner circle and outer part of linear polarizing film. Light from LEDs passes through the outer polarizing part, whereas the inner circle serves as a filter for light received by the camera lens. The distance between the camera lens and subject's face was about 0.7 m. All videos were

recorded at 39 frames per second with pixel resolution of 752 × 480 and saved frame-by-frame in a personal computer in the portable network graphic (PNG) format. Experiments were carried out in a darkened laboratory providing that the intensity of the LED illumination on the subject's face was at least ten times higher than the intensity of the ambient light. Each subject used eye protection goggles during video recording.

2.3. Signal processing

All recorded video frames from the cameras were processed off-line using custom software implemented in the MATLAB® platform. The core of the data processing algorithm was similar to that described in our previous work (Kamshilin *et al* 2018a). However, it was supplemented by estimation of instability of the PPG-waveform parameters. The algorithm consisted of the following steps.

2.3.1. Image stabilization.

For compensation of involuntary face motion during video recordings, all images were digitally stabilized. To this end, the image was divided on the segments of 64 × 30 pixels with independent compensation of each segment motion assuming that there are two time-varying components: PPG and the motion-related parts (Kamshilin et al 2018a). The motion-related component is proportional to the image gradient and lateral offset. The lateral offset was estimated in every segment by an optical flow algorithm using a gradient method (Kearney *et al* 1987). Thereafter, the motion-related signal component was reconstructed and subtracted from the original signal.

2.3.2. Selecting an area of analysis.

Considering previously reported observations of asymmetry and asynchronicity of facial blood flow (Zaproudina *et al* 2013), we analysed the difference in blood flow between the right and left sides of the subject's face. To this end, we manually determined a face symmetry line in one of the recorded images for each subject. Then, we selected an area for analysis exclusively on one (right) side of the face. An area for analysis on the left side was automatically covered by the same number of regions of interest (ROIs) as on the right side, but located mirrored with respect to the symmetry line. We used two types of ROIs (small and big) to estimate the parameters of facial blood flow. Small ROIs at a size of 5 × 5 pixels (that is about 1.5 × 1.5 mm^2 in the subject's face) covered the area of analysis so that adjacent ROIs had a common border without overlapping each other. In every small ROI we estimated two parameters of facial blood flow (a pulse arrival time, PAT, and an APC) using a previously published algorithm (Kamshilin *et al* 2018a). A typical example of mapping the PAT and APC parameters is shown in figure 1 for a subject from the control group. The dashed yellow line in figure 1 shows the symmetry line. One can see that both the PAT and APC are distributed unevenly over the facial area. To assess the statistics of blood-flow parameters, three big ROIs were selected in areas with elevated APC. These areas are usually located in the forehead and cheeks. The size of each big ROI was 8 × 8 small ROIs or about 12 × 12 mm^2. One ROI (the black square in figure 1) was manually selected in the forehead centre, and another (the red square in figure 1)—in the right cheek. The position of the third big ROI (the blue square in figure 1) was automatically defined as mirror-reflected with respect to the symmetry line. Assessment of the blood-flow asymmetry was performed by comparing the statistics of the blood-flow parameters in the red and blue big ROIs.

2.3.3. Statistics.

Statistical analysis was performed using the STATISTICA 10 software. To accept the null hypothesis, the differences between patient samples were evaluated in a comparative analysis for continuous variables using the nonparametric Mann–Whitney test and/or sign criterion. A nonparametric test is usually recommended for statistical analysis of continuous values for independent samples in a small population in which normality of distribution cannot be guaranteed. All continuous variables were expressed as the mean ± standard deviation (STD) of the mean. For the confidence limit, we took a confidence probability of $P > 0.05$.

2.3.4. PPG waveform and its instability.

In every small ROI, a raw waveform was estimated as frame-by-frame evolution of the average pixel value. As is known (Allen 2007), it consists of an alternating component (AC), which follows the heartbeat, and a slowly varying component (DC). Since both components are proportional to the incident light intensity, we compensated for illumination unevenness by calculating the AC/DC ratio. After subtracting the unity from the calculated ratio and inverting the sign, we obtained a waveform that correlates positively with variations in arterial blood pressure (Allen 2007, Kamshilin *et al* 2015). All the waveforms were filtered to remove noise and DC components by means of a zero-phase digital filter (0.12–20 Hz). Examples of the filtered PPG waveforms are shown in figure 2 for a patient with SSD (a) and a subject from the control group

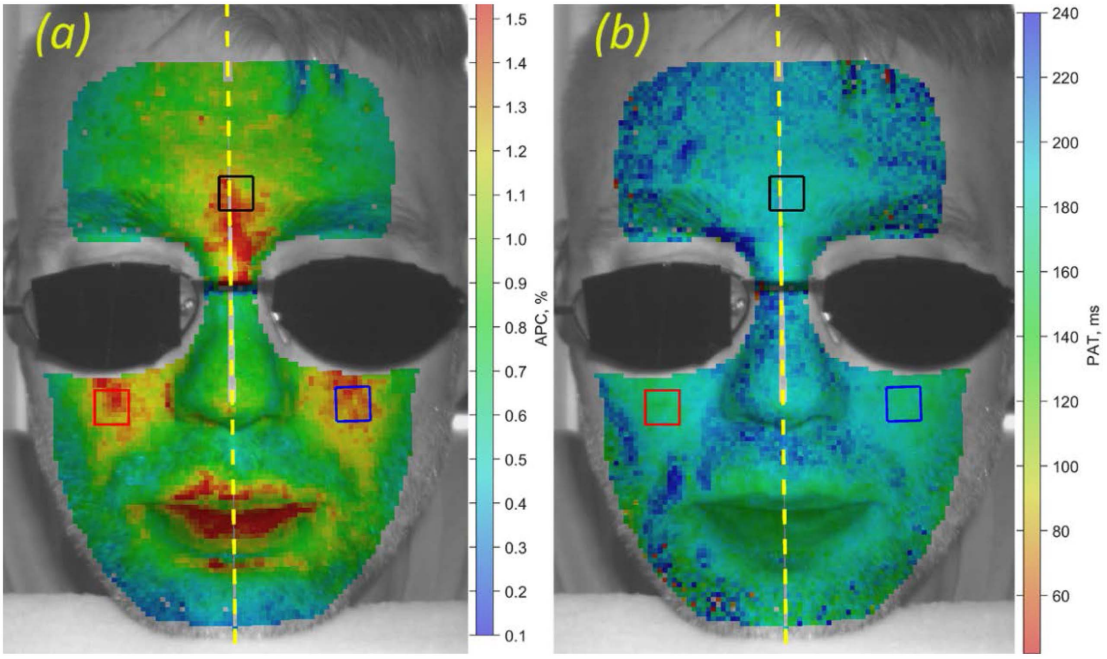

Figure 1. An example of selecting the area of analysis and spatial distributions of the blood-flow parameters overlaid with a still image of a subject from the control group. (a) Mapping the APC of PPG waveforms with the colour scale of this parameter in percent. (b) Mapping the PAT with the colour scale in milliseconds. The dashed yellow line shows the manually defined symmetry line of the face. Red, blue, and black squares show selected big ROIs for assessment of the APC and PAT.

(b). The lower graphs in figure 2 show respective ECG signals that were recorded simultaneously with video frames. It is worth noting that for clarity of presentation we limited the time scale in figure 2 by 2.5 s, whereas the duration of the recorded video was 40 s. Thin colour lines in the upper graphs in figure 2 show PPG waveforms calculated in different small ROIs within the big ROI in the left cheek. One can see that each PPG pulse follows the respective R-peak of the ECG signal. However, the pulses originating from adjacent small ROIs do not repeat one another, broadening presentation of the RRG waveforms in the graphs. As seen in figure 2, variations of the pulse shape are larger for the patient with SSD (panel a) than for the healthy subject (panel b). Note that all PPG waveforms in small ROIs were recorded simultaneously. Therefore, the observed variability of the pulses reflects their instability in space.

In addition to spatial variations of PPG pulses, we observed their instability in time: the shape of PPG pulses varies from one cardiac cycle to another. All these variations are caused by both physiological reasons and the uncertainty of the optical measurements. To illustrate the temporal instability of PPG pulses, we plotted together all pulses calculated in a representative small ROI (which was positioned inside the big ROI in the right cheek, as well) so that each respective R-peak of the ECG signal is at the beginning of the time scale. Depending on the heart rate, from 35 to 65 PPG pulses (their number is equal to the number of cardiac cycles) were assessed from 40 s of video. The PPG pulses are shown by thin coloured lines in figure 3(a) for a patient with SSD, and in figure 3(c) for a subject from the control group. It is clearly seen in figure 3 that the temporal instability of the PPG pulses is also higher in patients with SSD than in healthy subjects from the control group.

2.3.5. Assessment of PPG pulse parameters.

The graphs in figure 3 were used to illustrate the definition of the PPG-pulse parameters that we applied for quantitative comparison of the facial blood flow between patients with SSD and healthy subjects. First, we calculated a mean PPG pulse in each small ROI by averaging all cardiac-cycle waveforms (which are shown by thin coloured lines in figures 3(a) and (c)). Exemplary mean pulses for the patient with SSD and healthy subject are shown by thick greenish lines in figures 3(a) and (c), respectively. The parameter PAT was calculated in every small ROI as the time difference between the R-peak of the ECG and the minimum of the mean PPG pulse, which corresponds to the beginning of an anacrotic wave of the arterial blood pressure increase (Kamshilin *et al* 2018a). The APC was also estimated in every small ROI as the difference between the maximum and minimum values of the mean PPG pulse (see figures 3(a) and (c)). As an example, spatial distributions of the PAT and APC parameters overlaid with a still image of the subject's face are shown in figures 1(b) and (c), respectively. To assess asymmetry and unevenness of both the APC and PAT spatial

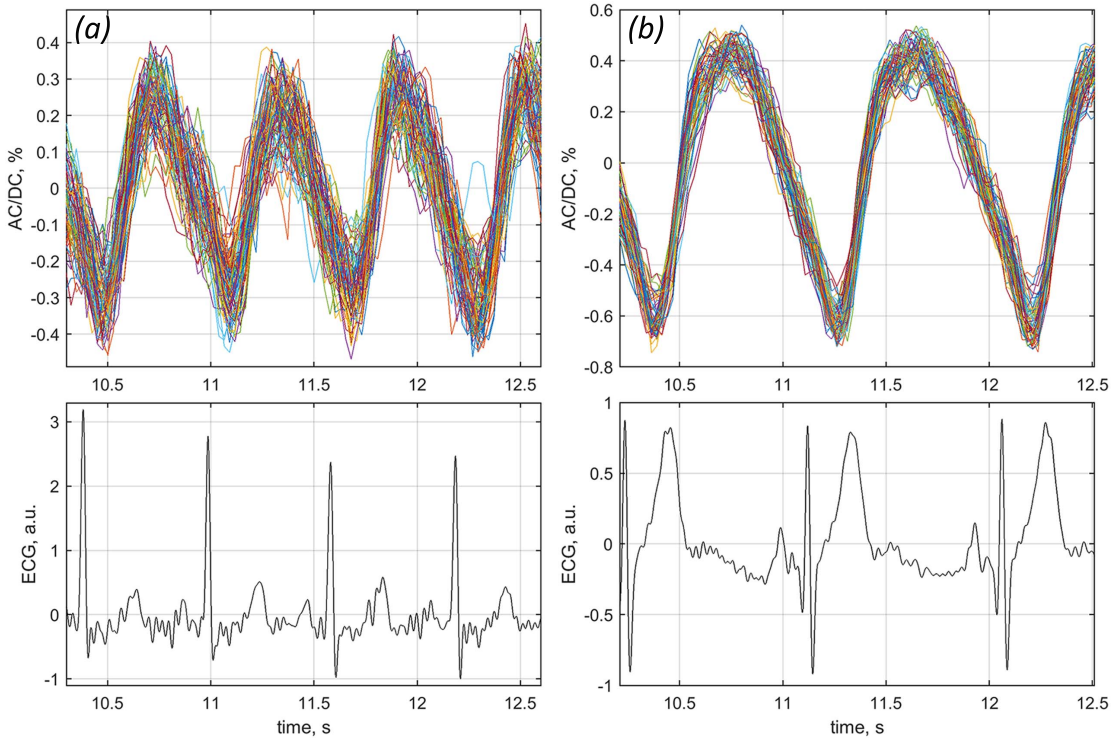

Figure 2. Instability of PPG pulses in space. Thin colour lines in the upper graphs show PPG waveforms assessed in 64 small ROIs situated within a big ROI in the right cheek (see figure 1). Video data were recorded simultaneously with ECG signals shown in the lower graphs. (a) PPG pulses and respective ECG measured for a patient with SSD. (b) PPG pulses and ECG for a subject from the control group.

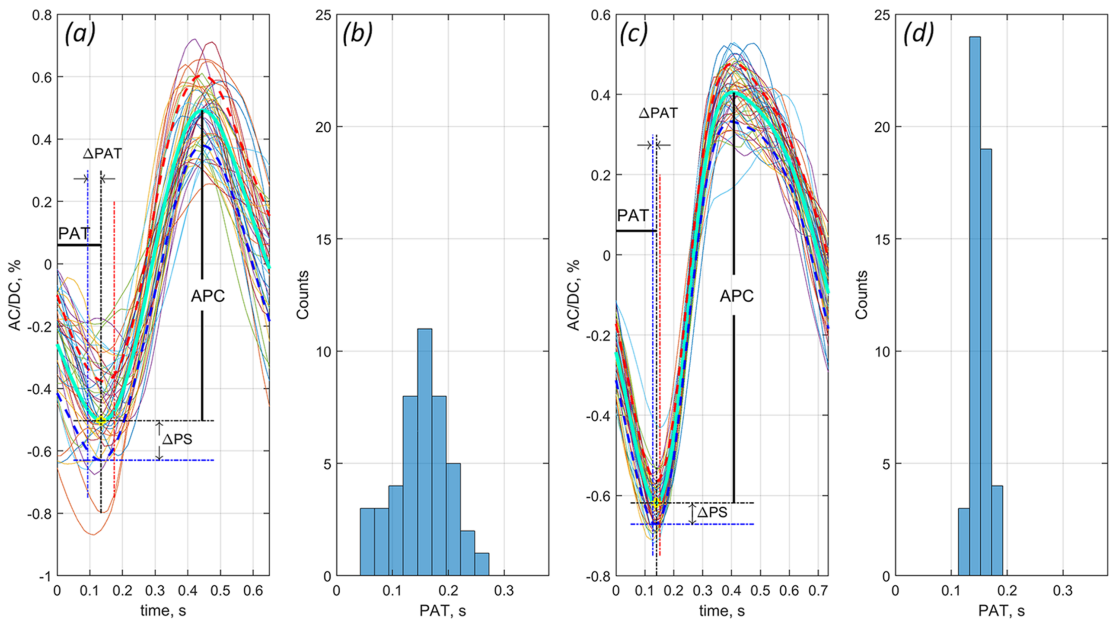

Figure 3. Instability of PPG pulses in time and a definition of PPG-waveform parameters. The thin coloured lines in graph (a) show PPG pulses of different cardiac cycles calculated in a small ROI situated in the right cheek of a patient with SSD. Panel (b) shows a histogram of the PAT estimated from 43 cardiac cycles of the patient with SSD. For comparison, PPG pulses of 48 cardiac cycles calculated in a small ROI for a subject from the control group are shown in panel (c), and the respective PAT histogram of these pulses is shown in panel (d). The thick greenish lines in (a) and (c) show the mean PPG pulses obtained after averaging of particular waveforms for the patient with SSD and healthy subject, respectively. The thick dashed red and blue lines in (a) and (c) are plotted as the mean $\pm$ STD of the pulses in each time point.

distribution, we evaluated their average magnitudes in three big ROIs selected in the cheeks and forehead. The degree of asymmetry was estimated as the modulus of the difference in the APC (or PAT) parameter averaged in the red and blue big ROIs, and normalized to their mean (in percent). In addition, the parameters averaged over the whole selected area and its right and left sides were estimated.

For quantitative evaluation of PPG-pulse instability, we adopted two parameters: variability of the PAT (ΔPAT), and pulse shape variability (ΔPS). Both ΔPAT and ΔPS were estimated in every small ROI within the chosen area of analysis. The ΔPAT was calculated as the STD of the PAT measured in each cardiac cycle during 40 s video recording:

$$\Delta PAT = \frac{1}{N-1}\sqrt{\sum_{i=1}^{N}\left(T_i - \overline{T}\right)^2}. \tag{1}$$

Here, N is the number of cardiac cycles, T_i is the PAT in i- cardiac cycle, and $\overline{T}$ is the PAT of the mean PPG pulse in a particular small ROI. The parameter ΔPAT is shown in figure 3(a) as the difference between black and blue vertical dash-dot lines that correspond to the PAT of the mean PPG pulse and STD of all particular pulses, respectively. To compare PAT variability between different patients and subjects, we used the ΔPAT averaged over 64 small ROIs within big ROIs in the right and left cheeks (marked by red and blue squares in figure 1). It was found that the mean ΔPAT in the cheeks is significantly smaller than the natural heart variability (HRV) evaluated from the synchronously recorded ECG as the STD of the cardiac cycles' durations. For an exemplary healthy subject, for which APC and PAT maps are shown in figure 1, HRV = 42.8 ms against $\Delta PAT = 14.3 \pm 2.1$ ms averaged over 64 small ROIs in the left cheek.

Pulse shape variability, ΔPS, was estimated as the STD of individual cardiac-cycle pulses from the mean PPG pulse (shown by thick greenish lines in figures 3(a) and (b)) with subsequent averaging of the STD values over all time points of the cardiac cycle:

$$\Delta PS = \frac{1}{M}\sum_{j=1}^{M}\left(\frac{1}{N-1}\sqrt{\sum_{i=1}^{N}\left(Y_{i,j} - \overline{Y_j}\right)^2}\right). \tag{2}$$

Here, M is the number of time points within one cardiac cycle (it was adopted to be $M = 64$ in our algorithm), N is the number of cardiac cycles (which is defined by the subject's heart rate), i and j are serial numbers of time samples and cardiac cycles, respectively, $Y_{i,j}$ is the magnitude of the PPG pulse of the i-cardiac cycle in the j- time point, and $\overline{Y_j}$ is the value of the mean PPG pulse in the j-time point. We illustrated the assessment of ΔPS in figure 3(a), where the mean PPG pulse is shown by the greenish thick curve, whereas the blue dashed curve shows the mean plus the STD of the individual pulses and the red dashed curve is the mean minus the STD of the pulses. Consequently, ΔPS is the mean distance between the solid greenish and dashed blue curves. As in the ΔPAT, we used averaging of the ΔPS over all small ROIs within red and blue big ROIs on the right and left cheeks while comparing pulse shape variability among patients and subjects.

3. Results

3.1. Mean PAT and APC in patients with SSD and control group

No significant difference in the mean APC was observed between the patients with SSD and control groups: $0.78 \pm 0.35\%$ and $0.91 \pm 0.28\%$ ($P = 0.20$), respectively. Similarity of the mean APC in patients and subjects is illustrated in figure 4, where this parameter is coded by pseudo-colours with the same scale for panels (a) and (b). As seen, the green colour prevails in both APC maps, which means approximately the same mean pulsation amplitude for the patient with SSD and the subject from the control group. Similarly, we did not find a significant difference in the mean PAT: 156 ± 19 ms for the patients versus 172 ± 49 ms for the control group, $P = 0.18$. Maps of the PAT are shown in figure 4 (panels (c) and (d) with the same colour-code scale) for the same patient and subject, respectively. Absence of a large difference in the colours of both distributions in panels (c) and (d) indicates an approximate equality of the average PAT in the exemplary patient and subject shown in figure 4.

However, our study revealed a significantly greater degree of asymmetry of the APC parameter in patients with scleroderma than in subjects from the control group: $17.7 \pm 9.7\%$ vs $7.9 \pm 5.0\%$, $P < 0.001$. One can clearly see in figure 4(a) that the APC of PPG waveforms in the left cheek of the patient with SSD is much higher than that in the right cheek: mean APC in the big blue ROI for this particular patient is $1.23 \pm 0.02\%$ vs $0.89 \pm 0.02\%$ ($P < 0.0001$). In contrast, the APC is almost symmetrically distributed on both cheeks of the subject from the control group: $0.85 \pm 0.03\%$ in the right cheek and $0.80 \pm 0.03\%$ in the left cheek, $P = 0.27$.

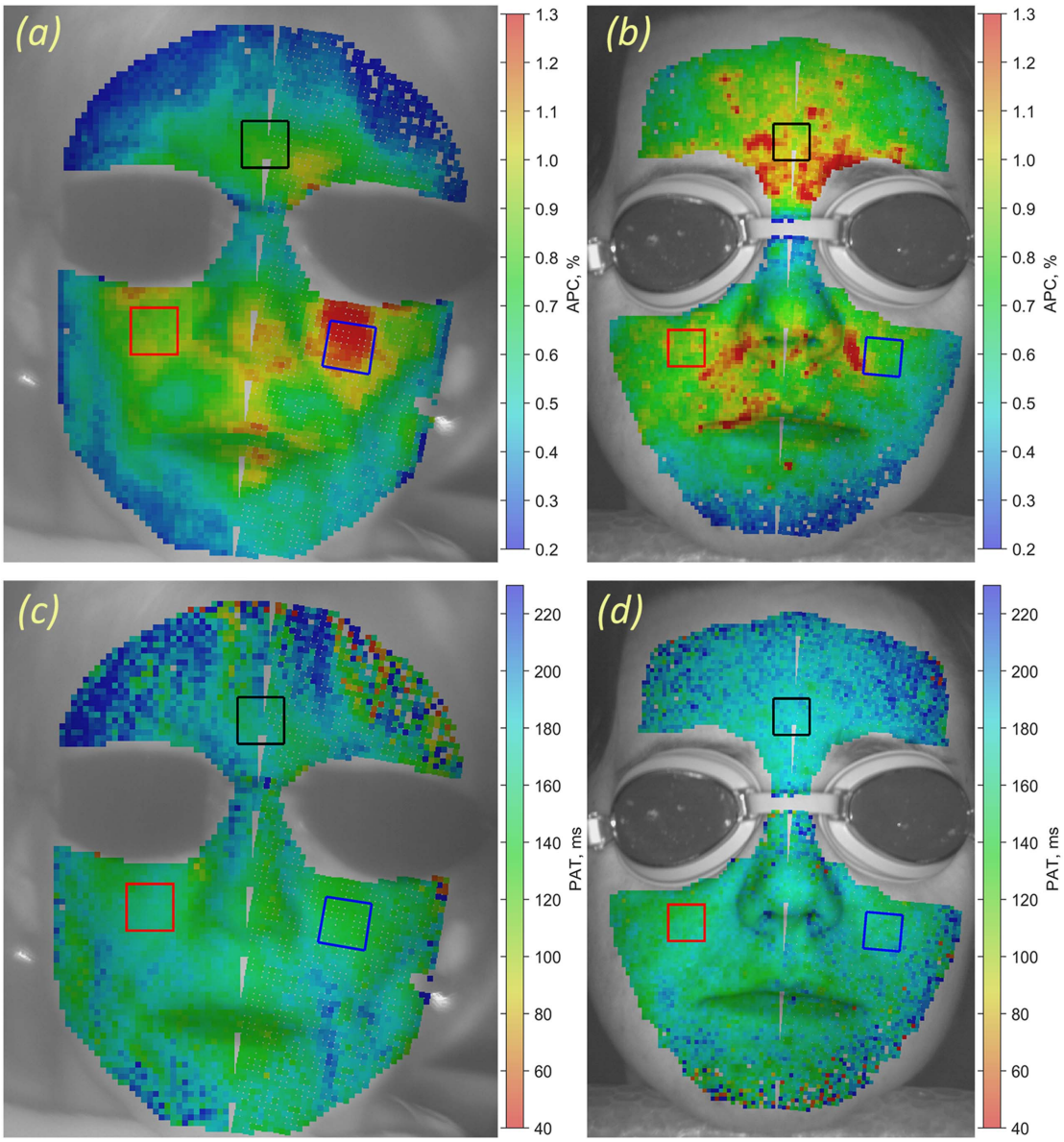

Figure 4. Maps of PPG parameters in facial areas. Spatial distribution of the APC for a patient with SSD (a) and a subject from the control group (b). Distribution of the PAT is shown in panels (c) and (d) for the same subjects, respectively.

3.2. Variability of the PPG waveforms parameters

In spite of the fact that our research has not revealed statistical distinction in the average APC and PAT values between groups of patients with SSD and the controls, the parameters describing variability of the blood flow in the facial area (ΔPAT and ΔPS) strongly differ between these groups. Analysis of the recorded data has revealed a significant increase in variability of both ΔPAT and ΔPS for patients with SSD. The ΔPAT in the right cheek (big red ROI) increased from 26 ± 16 ms to 57 ± 26 ms ($P = 0.006$) and from 23 ± 11 ms to 46 ± 45 ms ($P = 0.02$) in the left cheek (big blue ROI) for the control group and group of patients with SSD, respectively. No statistically significant difference in ΔPAT measured in the forehead (black big ROI) was found between these groups: 35 ± 25 ms versus 53 ± 47 ms, $P = 0.13$. The parameter ΔPS was larger in all three ROIs for patients with SSD compared to the control group: $0.14 \pm 0.07\%$ vs $0.09 \pm 0.03\%$ in the right cheek ($P = 0.002$); $0.12 \pm 0.06\%$ vs $0.08 \pm 0.02\%$ in the left cheek ($P = 0.008$); and $0.15 \pm 0.07\%$ vs $0.11 \pm 0.05\%$ in the forehead ($P = 0.03$). Comparison of the variability parameters between the patients and control group is shown in figure 5. While the increase in the ΔPAT was observed in each of the cheeks, an increase in the ΔPS was found in both the cheeks and forehead.

4. Discussion

The aim of our pilot study was to search for objective markers of microcirculatory disorders in patients with systemic scleroderma using the contactless IPPG technique at green illumination. In contrast to previous

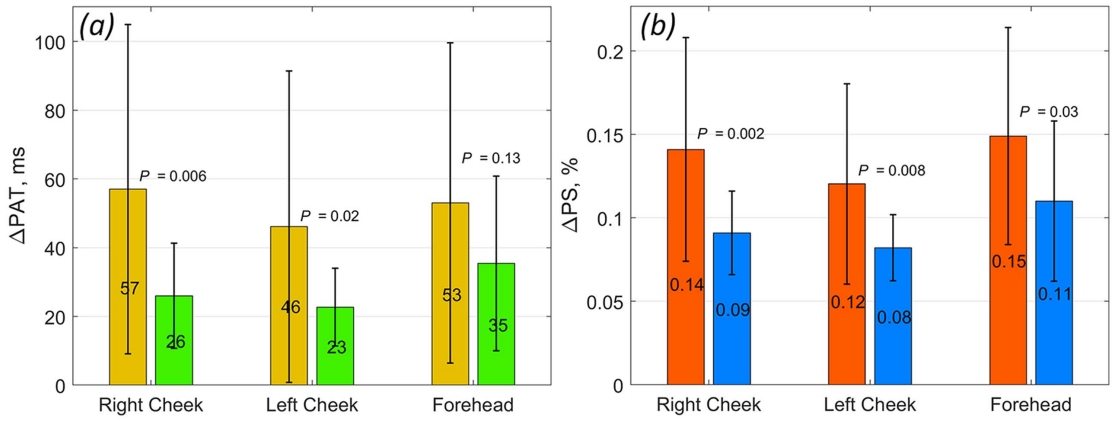

Figure 5. The increase in PPG pulse variability in patients with SSD compared to the control group: (a) ΔPTT parameter evaluated in patients with SSD (yellow bars) and in control subjects (green bars); (b) ΔPS parameter in patients with SSD (red bars) and in the control group (blue bars).

studies, which were conducted using the video-capillaroscopy method in the areas limited by the nailfold capillaries, we analysed blood-flow parameters in the facial area of patients with SSD for the first time. This favourably distinguishes the IPPG technique from the video-capillaroscopy that is capable of detecting changes in microcirculation only distal to the wrist joint (Ingegnoli *et al* 2018). Unlike in fingers, studying microcirculation in the facial area allows assessment of proximal skin lesions. We found two novel markers of sclerodermic skin lesions: (i) an increase in the variability of the pulse wave shape (ΔPS), and (ii) an increase in the variability of the PAT (ΔPAT). In addition, the degree of asymmetry in the amplitude of the PPG-wave pulsatile component was found to be larger in patients with SSD than in the control group.

It is worth noting that there is no difference in the quality of recorded PPG waveforms between patients with SSD and subjects from the control group. This is confirmed by the absence of a statistically significant difference in the APC between these groups, as well as by the example of the waveforms shown in figures 2 and 3. In the case of scleroderma, increased variability in the parameters is observed both in space (figure 2) and in time (figure 3). Evidently, these changes are directly related to the state of skin microcirculation thus affecting the parameters of the PPG waveform. We suggest that increased instability of PPG-pulse waves in patients with SSD is caused by a diminished number of functioning capillaries. According to the pathogenesis of the disease, it is accompanied by a violation of microcirculation in the background of endothelial dysfunction, as well as a significant decrease in the absolute number of surface capillaries in connection with autoimmune activation of fibroblasts (Furue *et al* 2017). In our IPPG system, the subject's skin was illuminated by green light. As is known (Anderson and Parrish 1981), this light has small penetration depth into the skin. According to the recently proposed model (Kamshilin *et al* 2015), in these conditions the PPG pulses are formed due to elastic deformations of the capillary bed: pulsatile variations in transmural blood pressure in arteries mechanically deform the interstitial tissue of the dermis that results in periodical changes in both absorption and scattering coefficients of the light in the upper layer of the skin. Recent study of capillary blood flow under the microscope has revealed significant differences in the shape of PPG waveforms originating from capillaries with running red blood cells and from connective tissue (Margaryants *et al* 2019). Therefore, it is likely that a PPG waveform averaged over a small ROI of the same size, but containing a smaller number of capillaries (as in patients with SSDs), might be more instable compared to the capillary bed of higher density (as in healthy subjects). However, the nature of this phenomenon remains not fully clarified and requires further in-depth study.

Considering successful assessment of micro-PPG parameters in arbitrary body regions (Margaryants *et al* 2019), we believe that the IPPG method will allow us to detect not only changes in blood flow in the face, but can also be a universal tool for diagnosing PSD, regardless of the region being evaluated.

At the same time we did not find any relationship between the severity of external manifestation of skin damage (Rodnan score) and parameters of the PPG waveform. On the one hand, this indicates differences in the nature of the compared parameters. On the other hand, it shows that the detected changes in PPG waveforms occur regardless of the appearance of dystrophic skin changes, possibly ahead of them.

There was also no relationship between variability of the PPG pulses and the disease duration. This observation gives us reason to classify the IPPG technique as an early diagnostic method that can be used to detect specific changes in capillary blood flow in the proximal skin areas in the early stages of the disease. This is especially important for improving treatment outcomes, the early onset of which can improve prognosis

and reduce patient disability (Volkmann *et al* 2014, Singh *et al* 2019). Considering the technique's simplicity and independence of the PPG-waveform-parameter changes on the disease duration, IPPG could find wide use in clinics, thus improving the quality of scleroderma diagnosis and making it more objective and reliable.

However, for confirmation of the obtained results, it is necessary to carry out the study in a wider patient population. Additionally, comparative analysis of PPG waveform changes in patients with scleroderma should be carried out in other body regions.

5. Conclusions

The method of IPPG is suitable for diagnosing PSD in the early stages of the disease. It is the variability of the PPG pulse shape which is changed most significantly in patients with SSD. Variability of the PAT and asymmetry of pulsations in the right and left cheeks are markers of the PSD as well. More considerable changes in indicators characterizing the instability of PPG waveforms are observed in patients with organ damage.

Acknowledgments

The Russian Science Foundation (Grant No. 15-15-20012) provided the financial support for this research. The authors have confirmed that any identifiable participants in this study have given their consent for publication.

ORCID iD

Alexei A Kamshilin https://orcid.org/0000-0003-2506-9736

References

Allen J 2007 Photoplethysmography and its application in clinical physiological measurement *Physiol. Meas.* **28** R1–39

Anderson R R and Parrish J A 1981 The optics of human skin *J. Invest. Dermatol.* **77** 13–19

Fett N 2013 Scleroderma: nomenclature, etiology, pathogenesis, prognosis, and treatments: facts and controversies *Clin. Dermatol.* **31** 432–7

Furue M, Mitoma C, Mitoma H, Tsuji G, Chiba T, Nakahara T, Uchi H and Kadono T 2017 Pathogenesis of systemic sclerosis-current concept and emerging treatments *Immunol. Res.* **65** 790–7

Ingegnoli F, Smith V, Sulli A and Cutolo M 2018 Capillaroscopy in routine diagnostics: potentials and limitations *Curr. Rheumatol. Rev.* **14** 5–11

Kamshilin A A, Krasnikova T V, Volynsky M A, Miridonov S V and Mamontov O V 2018a Alterations of blood pulsations parameters in carotid basin due to body position change *Sci. Rep.* **8** 13663

Kamshilin A A, Nippolainen E, Sidorov I S, Vasilev P V, Erofeev N P, Podolian N P and Romashko R V 2015 A new look at the essence of the imaging photoplethysmography *Sci. Rep.* **5** 10494

Kamshilin A A, Sidorov I S, Babayan L, Volynsky M A, Giniatullin R and Mamontov O V 2016 Accurate measurement of the pulse wave delay with imaging photoplethysmography *Biomed. Opt. Express* **7** 5138–47

Kamshilin A A, Volynsky M A, Khayrutdinova O, Nurkhametova D, Babayan L, Amelin A V, Mamontov O V and Giniatullin R 2018b Novel capsaicin-induced parameters of microcirculation in migraine patients revealed by imaging photoplethysmography *J. Headache Pain* **19** 43

Kearney J K, Thompson W B and Boley D L 1987 Optical flow estimation: an error analysis of gradient-based methods with local optimization *IEEE Trans. Pattern Anal. Mach. Intell.* **PAMI-9** 229–44

Leroy E C and Medsger T A Jr. 2001 Criteria for the classification of early systemic sclerosis *J. Rheumatol.* **28** 1573–6 (http://www.jrheum.org/content/28/7/1573)

Margaryants N B, Sidorov I S, Volkov M V, Gurov I P, Mamontov O V and Kamshilin A A 2019 Visualization of skin capillaries with moving red blood cells in arbitrary area of the body *Biomed. Opt. Express* **10** 4896–906

Poh M-Z, Mcduff D J and Picard R W 2010 Non-contact, automated cardiac pulse measurements using video imaging and blind source separation *Opt. Express* **18** 10762–74

Prakash S K A and Tucker C S 2018 Bounded Kalman filter method for motion-robust, non-contact heart rate estimation *Biomed. Opt. Express* **9** 873–97

Sidorov I S, Volynsky M A and Kamshilin A A 2016 Influence of polarization filtration on the information readout from pulsating blood vessels *Biomed. Opt. Express* **7** 2469–74

Singh D, Parihar A K S, Patel S, Srivastava S, Diwan P and Singh M R 2019 Scleroderma: an insight into causes, pathogenesis and treatment strategies *Pathophysiology* **26** 103–14 (https://www.sciencedirect.com/science/article/abs/pii/S0928468018303924)

van der Hoogen F *et al* 2013 Classification criteria for systemic sclerosis: an ACR-EULAR collaborative initiative *Arthritis Rheumatol.* **65** 2737–47

Volkmann E R *et al* 2014 Improved transplant-free survival in patients with systemic sclerosis-associated pulmonary hypertension and interstitial lung disease *Arthritis Rheumtol.* **66** 1900–8

Zaproudina N, Teplov V, Nippolainen E, Lipponen J A, Kamshilin A A, Närhi M, Karjalainen P A and Giniatullin R 2013 Asynchronicity of facial blood perfusion in migraine *PLoS One* **8** e80189